

# Quasi-periodic pulsations with multiple periods in hard X-ray emission

D. Li,<sup>1,2\*</sup> and Q. M. Zhang<sup>1</sup>

<sup>1</sup>Key Laboratory for Dark Matter and Space Science, Purple Mountain Observatory, CAS, Nanjing 210008, PR China

<sup>2</sup>Key Laboratory of Modern Astronomy and Astrophysics (Nanjing University), Ministry of Education, Nanjing 210023, PR China

Accepted XXX. Received YYY; in original form ZZZ

## ABSTRACT

We explore the quasi-periodic pulsations (QPPs) with multiple periods in hard X-ray (HXR) emission from *Fermi*/GBM during the impulsive phase of solar flare (SOL2014-09-10). The completely new observational result is that the shorter periods appear at lower energies of the X-ray photons at the beginning and the longer periods appear at higher energies at the end, with some intersection of the periods at medium energies. We also find the shorter and then the longer periods during the same phase of this flare. Using the wavelet power spectrum and fast Fourier transform (FFT) spectrum, we analyze the normalized rapidly varying signal divided by its slowly varying signal, which is the smoothed original HXR flux. The periods of 27 s and 37 s are derived at lower energy channels between 17:25 UT and 17:29 UT, i.e., 12.0–27.3 keV and 27.3–50.9 keV. Then the periods of 27 s, 46 s and 60 s are observed at medium-energy channel from 17:26 UT to 17:33 UT, such as 50.9–102.3 keV. And the period of 80 s is detected at higher energy channel from 17:28 UT to 17:33 UT, such as 102.3–296.4 keV.

**Key words:** Sun: flares – Sun: oscillations – Sun: X-rays, gamma-rays

## 1 INTRODUCTION

Quasi-periodic pulsations (QPPs) are usually observed in the light curves of solar flares (Nakariakov & Melnikov 2009; Inglis et al. 2016; Pugh et al. 2016; Van Doorselaere et al. 2016; Zhang et al. 2016a). They typically display regular and periodic peaks from the total flux based on the time-series analysis. The observations of QPPs can cover almost all the wavelengths, such as soft/hard X-rays (SXR/HXR) (Lipa 1978; Ning 2014; Aschwanden et al. 1998; Dolla et al. 2012; Tan et al. 2016), extreme-ultraviolet (EUV/UV) (Nakariakov et al. 1999; Ning & Guo 2014; Liu et al. 2011; Kumar et al. 2016; Li et al. 2016) and radio (Aschwanden et al. 1994; Ning et al. 2005; Tan et al. 2010; Yu et al. 2013; Kupriyanova et al. 2016) emission. In addition, QPPs can be detected with spectral observations, i.e., Doppler shifts, line widths and intensities (e.g., Ofman & Wang 2002; Wang et al. 2002; Tian et al. 2011; Brosius & Daw 2015; Li et al. 2015; Tian et al. 2016).

So far, it is still unclear which mechanism could cause the QPPs (Aschwanden et al. 1994; Nakariakov & Melnikov 2009; Van Doorselaere et al. 2016). Previous findings show that QPPs could be interpreted as the MHD wave (Roberts et al. 1984; Nakariakov & Verwichte 2005;

Nakariakov & Melnikov 2009; Tian et al. 2016) or produced by the quasi-periodic magnetic reconnection (Karlický et al. 2005; Nakariakov et al. 2006; Liu et al. 2011; Li et al. 2015; Li 2017). These QPPs models only apply to one or several events, but fail to explain all the observational features.

The observed periods of QPPs range from tens of seconds to tens of minutes (Lipa 1978; Aschwanden et al. 1994; Karlický et al. 2005; Tan et al. 2010; Shen & Liu 2012; Shen et al. 2013; Tan et al. 2016; Tian et al. 2016; Ning 2017). Sometimes, QPPs in the same event could show multiple periods in radio (Inglis & Nakariakov 2009), H $\alpha$  (Srivastava et al. 2008; Yang & Xiang 2016), EUV (Su et al. 2012), SXR (Chowdhury et al. 2015), and HXR (Zimovets & Struminsky 2010) bands. The period ratio of QPPs in the same event depends on the magnetohydrodynamic (MHD) mode (Nakariakov & Verwichte 2005). The ratio equals or almost equals two for the weakly dispersive MHD modes, i.e., torsion, slow magneto-acoustic, and kink. However, it deviates from two for the highly dispersive modes. The difference the period ratio from two is also attributed to additional physical effects like siphon flows (Li et al. 2013), the loop expansions (Verth & Erdélyi 2008), or the longitudinal density stratifications (Andries et al. 2005).

QPPs with multiple periods can be detected during all phases of solar flare, i.e., from impulsive to de-

\* E-mail: lidong@pmo.ac.cn

cay phases (Reznikova & Shibasaki 2011; Wang et al. 2012; Hayes et al. 2016; Tian et al. 2016). However, the fact that the dominant period of flare QPPs becomes longer with the increasing photon energy during the impulsive phase has not been reported yet. Using the high temporal resolution observations from *Fermi* Gamma-ray Burst Monitor (GBM) (Meegan et al. 2009), we explore the QPPs behaviors in a solar flare on 2014 September 10. The new observational finding may be a challenge to the QPPs theory, and could help to refine the model of flare QPPs.

## 2 OBSERVATIONS

In this paper, we investigate an X1.6 flare which takes place in NOAA AR 12158 on 2014 September 10. It is accompanied by a fast coronal mass ejection (CME) (Cheng & Ding 2016). It starts at about 17:21 UT, and then reaches its maximum at around 17:45 UT from the *GOES* SXR flux at 1.0–8.0 Å and 0.5–4.0 Å, respectively, as shown in Figure 1 (a). Figure 1 (b) shows the light curves at four HXR channels from *Fermi*/GBM, such as 12.0–27.3 keV, 27.3–50.9 keV, 50.9–102.3 keV, and 102.3–296.4 keV. To display the HXR light curves clearly, we have multiplied a factor for every HXR light curve. They are observed by n2 detector, whose direction angle to the Sun is relative stable during the impulsive phase of solar flare, i.e., between 17:21 UT and 17:45 UT. However, the other detectors frequently change their direction angles. After the impulsive phase (i.e., 17:45 UT), the n2 detector also shifts its direction angle frequently, this results into the HXR peak around 17:47 UT, which may be not real. It is missing data after 17:54 UT. The time cadence of *Fermi* light curves is about 0.256 s, but it automatically becomes to 0.064 s when the flare bursts. Therefore, the light curves from *Fermi* in Figure 1 (b) are interpolated into an uniform cadence, i.e., 0.256 s (see., Li et al. 2015; Ning 2017).

## 3 DATA REDUCTION TECHNIQUE

To look closely the periods of QPPs, we decompose every light curve into slowly varying signal and rapidly varying signal. The slowly varying signal is obtained by smoothing (SMOOTH.PRO in IDL) the original data with a timescale boxcar (Reznikova & Shibasaki 2011; Dolla et al. 2012; Li et al. 2015; Hayes et al. 2016), as shown by the dashed profile overlapping on the solid profile in Figure 1 (b). Previous observation has been suggested that this X1.6 flare may exhibit QPPs with short time periods in HXR bands, i.e., 30 s and 45 s (Ning 2017). However, these short timescale vibrations have much smaller amplitude than the strong background emission, which make them difficult to be detected (Dolla et al. 2012; Hayes et al. 2016). Therefore, the window timescale of 30 s is chosen to highlight the short timescale fluctuations. The rapidly varying signal is achieved by subtracting the slowly varying signal from its original light curve. And then the rapidly varying signal is normalized by its slowly varying signal, so that it could exhibit the QPPs behaviors much better (see., Kupriyanova et al. 2010, 2013; Li et al. 2017). Figure 2 (a) shows the normalized rapidly varying signal at HXR 12.0–27.3 keV between

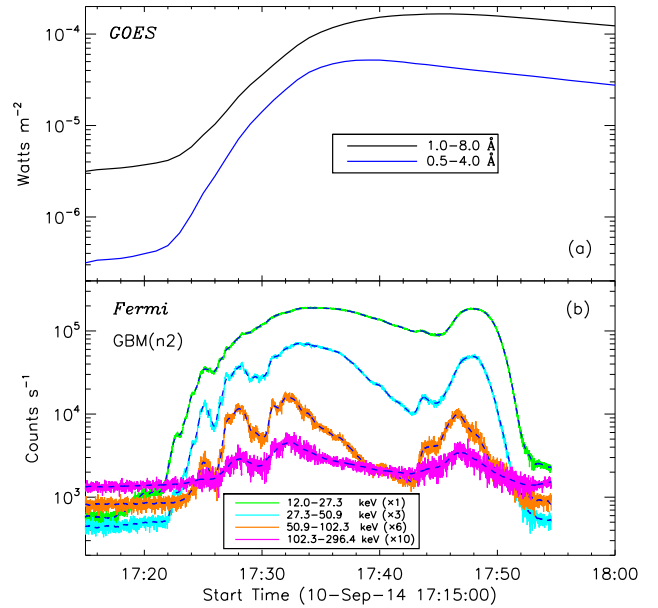


**Figure 1.** Panel (a): *GOES* SXR flux from 2014 September 10 flare at 1.0–8.0 Å (black) and 0.5–4.0 Å (blue). Panel (b): *Fermi* HXR light curves at 12.0–27.3 keV (green), 27.3–50.9 keV (turquoise), 50.9–102.3 keV (orange), and 102.3–296.4 keV (purple). The blue dashed profiles represent the slowly varying signals from original HXR light curves. Each HXR light curve is multiplying by a factor.

17:22 UT and 17:38 UT from *Fermi* observations. It clearly shows the periodic peaks and could be identified as QPPs. Note that we only select some time-series flux during the impulsive phase to avoid the frequently changing of the direction angle of n2 detector.

## 4 RESULTS OF ANALYSIS

Figure 2 (b) shows the wavelet power spectrum from the normalized rapidly varying signal at lower energy channel, i.e., 12.0–27.3 keV, the red contours outline the significance levels of 99.99%. It displays the dominant period with a broad band between 17:25 UT and 17:29 UT, as for most QPPs in microwave and HXR bands (Nakariakov & Melnikov 2009; Dolla et al. 2012; Hayes et al. 2016). To further confirm the periodicity, we perform a periodogram analysis for the normalized rapidly varying signal with the Lomb-Scargle periodogram method (Scargle 1982), as shown in panel (c). The red vertical line represents the 99.99% confidence level defined by Horne & Baliunas (1986). It shows two peaks above the confidence level, and both them have narrow widths. Therefore, the dominant period is obtained from the peak value in the Fourier periodogram, and the error bars are calculated from both the width of the spectral peak in the periodogram and the discreteness of the Fourier frequency grid. Thus two dominant periods within an error bar can be estimated from 17:25 UT to 17:29 UT at 12.0–27.3 keV, which are  $27 \pm 2.8$  s and  $37 \pm 3.5$  s. The same results can be found at 27.3–50.9 keV during almost the same time intervals, as seen in Figure 3. Although the wavelet spectrum still displays weak signal of periodicity after 17:29 UT (panel b), the

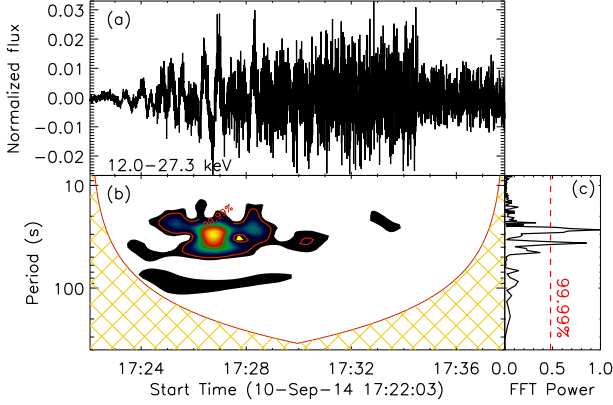


**Figure 2.** Panel (a): The normalized rapidly varying signal at 12.0–27.3 keV between 17:22 UT and 17:38 UT. Panel (b): Wavelet power spectrum. Panel (c): FFT spectrum. The red contours and vertical line outline the 99.99% confidence levels.

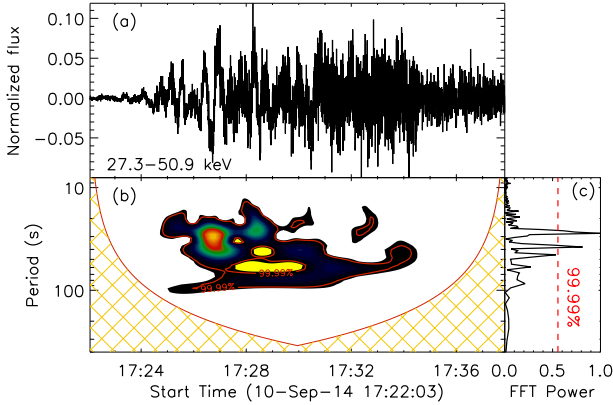


**Figure 3.** Same as Figure 2, but at 27.3–50.9 keV.

FFT spectrum only shows two peaks within narrow widths greater than the confidence level at about 27 s and 37 s, which are similar to that in Figure 2 (c). Thus we could derive the periods of  $27 \pm 2.8$  s and  $37 \pm 3.5$  s at 27.3–50.9 keV between 17:25 UT and 17:29 UT.

With the growth of HXR photon energies, the period of QPPs changes obviously to the larger value, as shown in Figures 4. At medium-energy channel (50.9–102.3 keV), the QPPs display multiple periods within a broad band from 17:26 UT to 17:33 UT. The shorter periods appear at the beginning of flare impulsive phase, such as between 17:26 UT and 17:29 UT. And the longer period appears at the end of flare impulsive phase, i.e., between 17:28 UT and 17:33 UT (Figure 4 b). Considering the peaks within narrow width in FFT spectrum, we can get three dominant periods within an error bar at 50.9–102.3 keV, they are  $27 \pm 1.8$  s,  $46 \pm 4.2$  s, and  $60 \pm 5.8$  s, as shown in Figure 4 (c).

At higher energy channel (102.3–296.4 keV), we apply a wider boxcar window of  $\sim 100$  s to smooth the light curve. Figure 5 (a) shows the normalized rapidly varying signal. The wavelet spectrum exhibits a period with a broad band between 17:28 UT and 17:33 UT, as shown in panel (b). However, the FFT spectrum only has one peak with a nar-

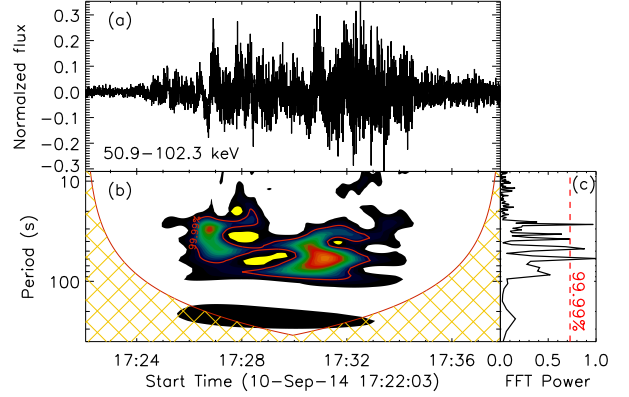


**Figure 4.** Same as Figure 2, but at 50.9–102.3 keV.

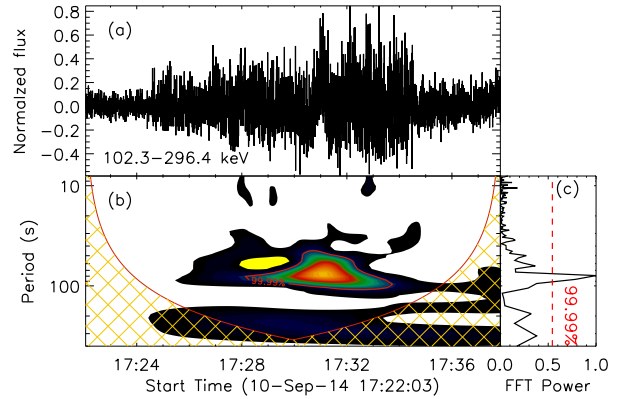


**Figure 5.** Same as Figure 2, but at 102.3–296.4 keV.

row width that greater than the confidence level, which is around 80 s. Based on these facts, we could obtain the dominant period within an error bar of  $80 \pm 11$  s at higher energy channel. Even if using the short window timescale ( $\sim 30$  s), we could not find any periodic signal with shorter period at higher energy channel. In other words, QPPs with shorter period are only observed at lower energy channels, but fail to be detected at higher energy channel.

## 5 DISCUSSIONS

It is very interesting that the flare QPPs display multiple periods in HXR emission during the impulsive phase of solar flare, and the shorter periods tend to appear at lower energies of the X-ray photons, while the longer periods appear at higher energies, with some intersection of the periods at medium energies. The periods are 27 s and 37 s at lower photon energies (Figures 2 and 3), and become around 80 s at higher photon energies (Figure 5). Then the periods of 27 s, 46 s and 60 s are found at medium photon energies (Figure 4). To our knowledge, this is the first report that the QPPs display their dominant periods become longer with the increasing of the photon energies in HXR emission. Previous observations have reported the various periods in multi-wavelengths. For exam-

ple, [Zimovets & Struminsky \(2010\)](#) report 16 s and 36 s QPPs at SXR and HXR channels (*RHESSI*, 3–50 keV). [Su et al. \(2012\)](#) detect flare QPPs with periods of 24–160 s at EUV band (AIA 171 Å). [Chowdhury et al. \(2015\)](#) investigate QPPs during the decay phase of solar flare and find double periods of ~53 s and ~72 s at SXR channels (*RHESSI*, 3–25 keV). However, these observations just report the multiple periods at one or several bands, but not indicate the periods changing with the photon energies. Another interesting thing is that the flare QPPs show their multiple periods appear at different times during the impulsive phase of solar flare. This is also a new result comparing with previous findings about multi-period QPPs. For example, [Reznikova & Shibasaki \(2011\)](#) find that the periods become longer continuously in the nonthermal emission. [Hayes et al. \(2016\)](#) and [Tian et al. \(2016\)](#) detect the different periods during the flare impulsive and decay phases, respectively.

It is also interesting that the flare QPPs show the period ratio within several values at HXR channels. At lower photon energies, the period ratio is estimated to about 1.37 from the two dominant periods; and at medium photon energy, the period ratios are around 2.22, 1.70 and 1.30, while at higher photon energy, there is only one period value. On the other hand, the period ratio between different photon energies can also be calculated. For example, the period ratios are 2.96 and 2.16 between higher and lower photon energies, and the period ratios of around 2.96, 1.74 and 1.33 can be detected between higher and medium photon energies. The period ratios between medium and lower photon energies are much more and complex, since both of them display several dominant periods. Similar as previous findings ([Srivastava et al. 2008](#); [Inglis & Nakariakov 2009](#); [Su et al. 2012](#); [Tian et al. 2016](#); [Yang & Xiang 2016](#)), all these period ratios are deviating from two. This may be due to the expansion of flare loop ([Verth & Erdélyi 2008](#)), or the density stratification in solar flare ([Andries et al. 2005](#)).

The X1.6 flare on 2014 September 10 also exhibits QPPs with multiple periods at various wavelengths, such as ~240 s QPPs at HXR, EUV/UV and radio emission ([Li & Zhang 2015](#); [Li et al. 2015](#); [Dudík et al. 2016](#)), ~120 s and ~60 s QPPs at SXR/HXR and EUV/UV bands ([Ning 2017](#)). In this paper, we obtain the multiple periods in HXR emission, i.e., 27 s, 37 s, 46 s, 60 s and 80 s. The different periods of the flare QPPs in pervious findings ([Li et al. 2015](#); [Ning 2017](#)) are derived from the different rapidly varying signals, which are dependent on the window timescale. The window timescale of ~240 s QPPs is 256 s ([Li et al. 2015](#)), and that of ~60 s QPPs is 100 s ([Ning 2017](#)). Both these QPPs can last up to around 18:00 UT at EUV/UV bands, which is the decay phase of solar flare ([Li et al. 2015](#); [Ning 2017](#)). Different from these previous observations, we find the shorter and then the longer periods during the impulsive phase of this flare.

It is well known that the X-ray emission at lower and higher photon energies can be produced by different mechanisms, i.e., by thermal plasmas or by nonthermal electron beams. Usually, the thermal component is extended up to 20 keV ([Ning 2008](#); [Zhang et al. 2016b](#)). And sometimes, the nonthermal component can also be as low as about 10 keV ([Krucker et al. 2002](#); [Ning 2007, 2008](#)). Therefore, the longer periods at medium and higher photon energies are produced

by accelerated particles. And the shorter periods at lower photon energies (12.0–27.3 keV) seem to be produced by thermal plasmas. However, we could not find the shorter periods at 4.6–12.0 keV, and the shorter periods can also be detected at 27.3–50.9 keV. This is an indirect evidence that the QPPs are the features of nonthermal emission. In a word, all the periods of flare QPPs in X-ray emission during the impulsive phase of solar flare may be produced by nonthermal electron beams. Meanwhile, fitting the energy spectrum could proof this hypothesis, but it is out of scope of this paper.

## ACKNOWLEDGEMENTS

The authors would like to thank the anonymous referee for his/her valuable comments that improved the manuscript. We thank the teams of *Fermi* and *GOES* for their open data use policy. This study is supported by NSFC under grants 11603077, 11573072, 11333009, 973 program (2014CB744200), and Laboratory No. 2010DP173032. D. Li is supported by the Youth Fund of Jiangsu No. BK20161095. Q. M. Zhang is supported by the Surface Project of Jiangsu No. BK20161618 and the Youth Innovation Promotion Association CAS. The authors wish to thank the International Space Science Institute in Beijing (ISSI-BJ) for supporting and hosting the meetings of the International Team on “Magnetohydrodynamic Seismology of the Solar Corona in the Era of SDO/AIA”, during which the discussions leading to this publication were held.

## REFERENCES

- Andries, J., Arregui, I., & Goossens, M. 2005, *ApJ*, 624, L57  
 Aschwanden, M. J., Benz, A. O., Dennis, B. R., & Kundu, M. R. 1994, *ApJS*, 90, 631  
 Aschwanden, M. J., Kliem, B., Schwarz, U., et al. 1998, *ApJ*, 505, 941  
 Brosius, J. W., & Daw, A. N. 2015, *ApJ*, 810, 45  
 Cheng, X., & Ding, M. D. 2016, *ApJ*, 823, L4  
 Chowdhury, P., Srivastava, A. K., Dwivedi, B. N., Sych, R., & Moon, Y.-J. 2015, *Advances in Space Research*, 56, 2769  
 Dudík, J., Polito, V., Janvier, M., et al. 2016, *ApJ*, 823, 41  
 Dolla, L., Marqué, C., Seaton, D. B., et al. 2012, *ApJ*, 749, L16  
 Hayes, L. A., Gallagher, P. T., Dennis, B. R., et al. 2016, *ApJ*, 827, L30  
 Horne, J. H., & Baliunas, S. L. 1986, *ApJ*, 302, 757  
 Inglis, A. R., & Nakariakov, V. M. 2009, *A&A*, 493, 259  
 Inglis, A. R., Ireland, J., Dennis, B. R., Hayes, L., & Gallagher, P. 2016, *ApJ*, 833, 284  
 Karlický, M., Bárta, M., Mészáros, H., & Zlobec, P. 2005, *A&A*, 432, 705  
 Krucker, S., Christe, S., Lin, R. P., Hurford, G. J., & Schwartz, R. A. 2002, *Sol. Phys.*, 210, 445  
 Kumar, P., Nakariakov, V. M., & Cho, K.-S. 2016, *ApJ*, 822, 7  
 Kupriyanova, E. G., Melnikov, V. F., Nakariakov, V. M., & Shibasaki, K. 2010, *Sol. Phys.*, 267, 329  
 Kupriyanova, E. G., Melnikov, V. F., & Shibasaki, K. 2013, *Sol. Phys.*, 284, 559  
 Kupriyanova, E. G., Kashapova, L. K., Reid, H. A. S., & Myagkova, I. N. 2016, *Sol. Phys.*, 291, 3427  
 Li, B., Habbal, S. R., & Chen, Y. 2013, *ApJ*, 767, 169  
 Li, D., Ning, Z. J., & Zhang, Q. M. 2015, *ApJ*, 807, 72  
 Li, D. 2017, *Research in Astronomy and Astrophysics*, 17, 040

- Li, D., Zhang, Q. M., Huang, Y., Ning, Z. J., & Su, Y. N. 2017, *A&A*, 597, L4
- Li, L. P., Zhang, J., Su, J. T., & Liu, Y. 2016, *ApJ*, 829, L33
- Li, T., & Zhang, J. 2015, *ApJ*, 804, L8
- Lipa, B. 1978, *Sol. Phys.*, 57, 191
- Liu, W., Title, A. M., Zhao, J., et al. 2011, *ApJ*, 736, L13
- Meegan, C., Lichti, G., Bhat, P. N., et al. 2009, *ApJ*, 702, 791-804
- Nakariakov, V. M., Ofman, L., Deluca, E. E., Roberts, B., & Davila, J. M. 1999, *Science*, 285, 862
- Nakariakov, V. M., & Verwichte, E. 2005, *Living Reviews in Solar Physics*, 2, 3
- Nakariakov, V. M., Foullon, C., Verwichte, E., & Young, N. P. 2006, *A&A*, 452, 343
- Nakariakov, V. M., & Melnikov, V. F. 2009, *Space Sci. Rev.*, 149, 119
- Ning, Z., Ding, M. D., Wu, H. A., Xu, F. Y., & Meng, X. 2005, *A&A*, 437, 691
- Ning, Z. 2007, *ApJ*, 659, L69
- Ning, Z. 2008, *ApJ*, 686, 674-685
- Ning, Z. 2014, *Sol. Phys.*, 289, 1239
- Ning, Z., & Guo, Y. 2014, *ApJ*, 794, 79
- Ning, Z. 2017, *Sol. Phys.*, 292, 11
- Ofman, L., & Wang, T. 2002, *ApJ*, 580, L85
- Pugh, C. E., Armstrong, D. J., Nakariakov, V. M., & Broomhall, A.-M. 2016, *MNRAS*, 459, 3659
- Reznikova, V. E., & Shibasaki, K. 2011, *A&A*, 525, A112
- Roberts, B., Edwin, P. M., & Benz, A. O. 1984, *ApJ*, 279, 857
- Scargle, J. D. 1982, *ApJ*, 263, 835
- Shen, Y., & Liu, Y. 2012, *ApJ*, 753, 53
- Shen, Y.-D., Liu, Y., Su, J.-T., et al. 2013, *Sol. Phys.*, 288, 585
- Srivastava, A. K., Zaqarashvili, T. V., Uddin, W., Dwivedi, B. N., & Kumar, P. 2008, *MNRAS*, 388, 1899
- Su, J. T., Shen, Y. D., Liu, Y., Liu, Y., & Mao, X. J. 2012, *ApJ*, 755, 113
- Tan, B., Zhang, Y., Tan, C., & Liu, Y. 2010, *ApJ*, 723, 25
- Tan, B., Yu, Z., Huang, J., Tan, C., & Zhang, Y. 2016, *ApJ*, 833, 206
- Tian, H., McIntosh, S. W., & De Pontieu, B. 2011, *ApJ*, 727, L37
- Tian, H., Young, P. R., Reeves, K. K., et al. 2016, *ApJ*, 823, L16
- Wang, T., Solanki, S. K., Curdt, W., Innes, D. E., & Dammasch, I. E. 2002, *ApJ*, 574, L101
- Wang, T., Ofman, L., Davila, J. M., & Su, Y. 2012, *ApJ*, 751, L27
- Van Doorsselaere, T., Kupriyanova, E. G., & Yuan, D. 2016, *Sol. Phys.*, 291, 3143
- Verth, G., & Erdélyi, R. 2008, *A&A*, 486, 1015
- Yang, S., & Xiang, Y. 2016, *ApJ*, 819, L24
- Yu, S., Nakariakov, V. M., Selzer, L. A., Tan, B., & Yan, Y. 2013, *ApJ*, 777, 159
- Zhang, Q. M., Li, D., & Ning, Z. J. 2016a, *ApJ*, 832, 65
- Zhang, Q. M., Li, D., Ning, Z. J., et al. 2016b, *ApJ*, 827, 27
- Zimovets, I. V., & Struminsky, A. B. 2010, *Sol. Phys.*, 263, 163

This paper has been typeset from a  $\text{\TeX}/\text{\LaTeX}$  file prepared by the author.